AD_____

CONTRACT NUMBER DAMD17-96-C-6035

TITLE: Biological Sensors and Multiorgan Diagnostic Screening Physiographic Personnel Monitor

PRINCIPAL INVESTIGATOR: Dr. Martin C. Baruch

CONTRACTING ORGANIZATION: Empirical Technologies Corporation
Charlottesville, Virginia 22902

REPORT DATE: October 1996

TYPE OF REPORT: Final, Phase I

PREPARED FOR: Commander
U.S. Army Medical Research and Materiel Command
Fort Detrick, Frederick, Maryland 21702-5012

REPORT DOCUMENTATION PAGE

Form Approved
OMB No. 0704-0188

1. AGENCY USE ONLY *(Leave blank)*	2. REPORT DATE	3. REPORT TYPE AND DATES COVERED
	October 1996	Final, Phase I (28 Mar 96-27 Sep 96)

4. TITLE AND SUBTITLE
Biological Sensors and Multiorgan Diagnostic Screening Physiographic Personnel Monitor

5. FUNDING NUMBERS
DAMD17-96-C-6035

6. AUTHOR(S)
Dr. Martin C. Baruch
Dr. Charles M. Adkins
Dr. David W. Gerdt

7. PERFORMING ORGANIZATION NAME(S) AND ADDRESS(ES)
Empirical Technologies Corporation
Charlottesville, Virginia 22902

8. PERFORMING ORGANIZATION REPORT NUMBER

9. SPONSORING/MONITORING AGENCY NAME(S) AND ADDRESS(ES)
Commander
U.S. Army Medical Research and Materiel Command
Fort Detrick, Frederick, MD 21702-5012

10. SPONSORING/MONITORING AGENCY REPORT NUMBER

11. SUPPLEMENTARY NOTES

12a. DISTRIBUTION / AVAILABILITY STATEMENT
Approved for public release; distribution unlimited

12b. DISTRIBUTION CODE

13. ABSTRACT *(Maximum 200)*

The Phase I effort has established the feasibility of a heartbeat and respiration sensor with high sensitivity, based on a fiber optic coupler that will fit within the dimensions of a wrist watch. Radio fequency transmission tests have demonstrated the feasibility of using a custom designed IC with on-board antenna and driver circuitry to transmit the sensor's low frequency signal to a receiver unit over a distance o f one meter or more at frequencies of 220 - 420 MHz. Electronic interface units were constructed that contain the circuitry necessary for opto-electronic conversion as well as to perform the sum and difference calculations to isolate the heartbeat-related chnages in the sensor's output signal. A laptop-based A/D data acquisition system was implemented.

14. SUBJECT TERMS
fiber optic, coupler, sensor, transmission
radio frequency, integrated circuit, heart beat, respiration

15. NUMBER OF PAGES
23

16. PRICE CODE

17. SECURITY CLASSIFICATION OF REPORT	18. SECURITY CLASSIFICATION OF THIS PAGE	19. SECURITY CLASSIFICATION OF ABSTRACT	20. LIMITATION OF ABSTRACT
Unclassified	Unclassified	Unclassified	Unlimited

FOREWORD

Opinions, interpretations, conclusions and recommendations are those of the author and are not necessarily endorsed by the U.S. Army.

____ Where copyrighted material is quoted, permission has been obtained to use such material.

____ Where material from documents designated for limited distribution is quoted, permission has been obtained to use the material.

____ Citations of commercial organizations and trade names in this report do not constitute an official Department of Army endorsement or approval of the products or services of these organizations.

____ In conducting research using animals, the investigator(s) adhered to the "Guide for the Care and Use of Laboratory Animals," prepared by the Committee on Care and use of Laboratory Animals of the Institute of Laboratory Resources, national Research Council (NIH Publication No. 86-23, Revised 1985).

____ For the protection of human subjects, the investigator(s) adhered to policies of applicable Federal Law 45 CFR 46.

____ In conducting research utilizing recombinant DNA technology, the investigator(s) adhered to current guidelines promulgated by the National Institutes of Health.

____ In the conduct of research utilizing recombinant DNA, the investigator(s) adhered to the NIH Guidelines for Research Involving Recombinant DNA Molecules.

____ In the conduct of research involving hazardous organisms, the investigator(s) adhered to the CDC-NIH Guide for Biosafety in Microbiological and Biomedical Laboratories.

PI - Signature 10/17/96 Date

Table of Contents:

Introduction

The purpose of this program was to demonstrate the feasibility of a fiber-optic coupler-based heartbeat and respiration sensor which is compact and portable. The sensor device was a single mode fiber optic coupler whose coupling ratio was highly sensitive to small bending moments, such as are caused by skin deflections due to pulse pressure. Changes in the coupling ratio of the light traversing the coupler were measured by photodiodes on each of the fiber coupler's two outputs. The diodes' electronic signal was recorded and analyzed.

The Phase I technical objective was to demonstrate a 'proof of principle' engineering model of a fiber optic sensor system for detection of various physiographic states or disorders which are available through monitoring of the heartbeat, pulse, or breathing rate of personnel in critical situations. The physical parts of the system encompassed the sensor, the light source and its driver, the photodiodes and their supporting electronics, as well as a data logger.

Five tasks were outlined in the Statement of Work to develop and demonstrate the system capabilities. All five tasks were completed in the course of the program. Task 1 ("Coupler sensors will be constructed ... ") involved the actual construction of fiber optic couplers and their implementation as sensors by mounting them in support frames of different geometries. Several designs were tried and the development of the sensor geometry over the course of the program was quite remarkable, resulting in a device of substantially reduced size and enhanced sensitivity and ruggedization. Task 2 ("Transition to 1300 nm LEDs") was originally proposed due to the noticeably lower costs of operating at that wavelength, since both light sources and fiber can be obtained comparably cheaply due to the high production volume required by the communications industry. Noise analyses were performed to determine the tradeoffs of using LED versus laser sources in order to control noise and enhance the signal to noise ratio in the very low frequency passband appropriate for heart, breathing, and body motions. Task 3 ("Design and construct several Electronic Interface Units") involved the design, construction and testing of an electronic package consisting of an LED controller chip, photodiodes, as well as transimpedance amplifiers and an instrumentation amplifier to convert the optical signal and enhance the signal to noise ratio. A noise analysis was performed on the design, and its performance is in accordance with predictions. Task 4 ("Data logger interface ... ") mainly involved the interface of a computer with the EIU through an analog/digital conversion board. A notebook computer was programmed in the Windows © environment to perform this task. A description of the program as well as pertinent sections of the code are given. Radio transmission experiments were performed in order to test the feasibility of transmitting signals from the sensor package to the logger. In the context of Task 5 ("Test of the heartbeat/respiration sensor") a number of data streams were obtained from team members, demonstrating the capability of the fiber optic sensor to record heart beat and respiration signals of high spectral purity. Spectral analysis using FFTs were performed in order to determine the spectral content of the

signal, which in turn determined the digital acquisition rates and filter roll-offs in the electronic circuitry.

Program Results

The fiber optic sensor described in this report is a variation of the "fused biconical tapered coupler" which has been developed extensively for the telecommunications market to enable optical signals to be extracted from or added to an optical fiber trunk. The coupler is a four terminal device formed by fusing single mode optical fibers in a furnace or flame and pulling or drawing the fused region until the fibers are very small (about 15 μm), closely spaced, and parallel. Light inserted into one of the four leads, will split into the two downstream fibers with a power distribution which is described in terms of the coupling ratio (power coupled into the other fiber / total power input) .

Used as a sensor, there are several "measurands" which can be used to vary the coupling ratio. Among these are the wavelength of the injected light, the index of refraction of the environment surrounding the coupler, and bending of the fused "waist region" of the two couplers. This effect was developed and patented by Gerdt and Gilligan.[1] The patent assignee is Sperry Marine, Inc. of Charlottesville, Virginia. ETC is exploiting the characteristics of the fiber optic coupler sensor under license to Sperry.

Several authors have proposed models for the bending response of the fiber optic coupler [234], however due to the significant degree of bending which has been used, the theoretical models proposed are not very instructive for design guidance.

TASK 1 -- "Coupler sensors will be constructed and the leads will be directly integrated with a fiber optic pigtailed LED and two pigtailed detectors:"

The original experiments on this program repeated the construction of the first sensor configuration which had been used by Gerdt, et.al. for detection of sonar signals for NADC [5] and NUSC [6]. This design, in its simplest form simply embedded a taught fiber optic coupler in a membrane of GE RTV 12 (GE RTV 8111A or Dow Corning Sylguard could also be used with identical results). The two inch diameter membrane was housed in a 1/8 in. thick plexiglas frame which supported the membrane and the fibet. Fiber ends were secured using epoxy to the Plexiglas housing. Light input was provided by splicing the output fiber from a pigtailed Light Emitting Diode or Laser Diode to one of the input lines for the embedded coupler. The two output lines were fed to a pair of germanium detectors and transimpedance amplifiers. Pressure or force applied against the membrane caused it to deflect, bending the fiber, and causing a noticeable change in the coupling ratio. This configuration is illustrated in Figure 1.

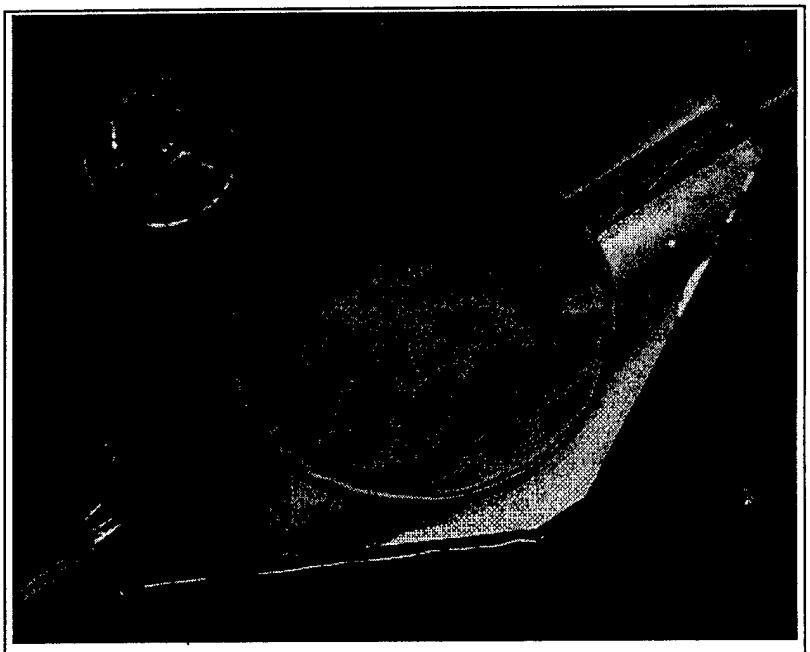

Figure 1 The Original Fiber Optic Sensor in Plexiglas Housing

The original configuration always produced a significant signal output as the membrane was deformed, however sometimes the shift occurred because of variations in propagation loss (both fibers produced the same signal) and sometimes the shift occurred because of variation in coupling ratio (the signals in the two fibers were complementary). In addition, the package was large (about 4 in. x 3 in. with a 2 inch diameter membrane) and fragile because the fiber was physically stretched as the membrane deformed. For these reasons, a new configuration was sought which would produce a reliably predictable output variation derived from a given measurand.

A second set of experiments was designed by which the bending response of the coupler itself could be measured and compared with the somewhat qualitative observations made with the original coupler design. For these experiments, couplers were drawn on the fabrication bench and physically bent around a 4 mm clean glass rod which imposed a fixed radius of curvature in the deformed region. During the experiment an axial tension of about 2 grams was maintained on the fiber ends to insure that the fiber remained taut and that bending was limited to the intended location. A typical result is illustrated in Figure 2.

The results of these experiments were instructive and guided the development of the sensing device. The observations were:

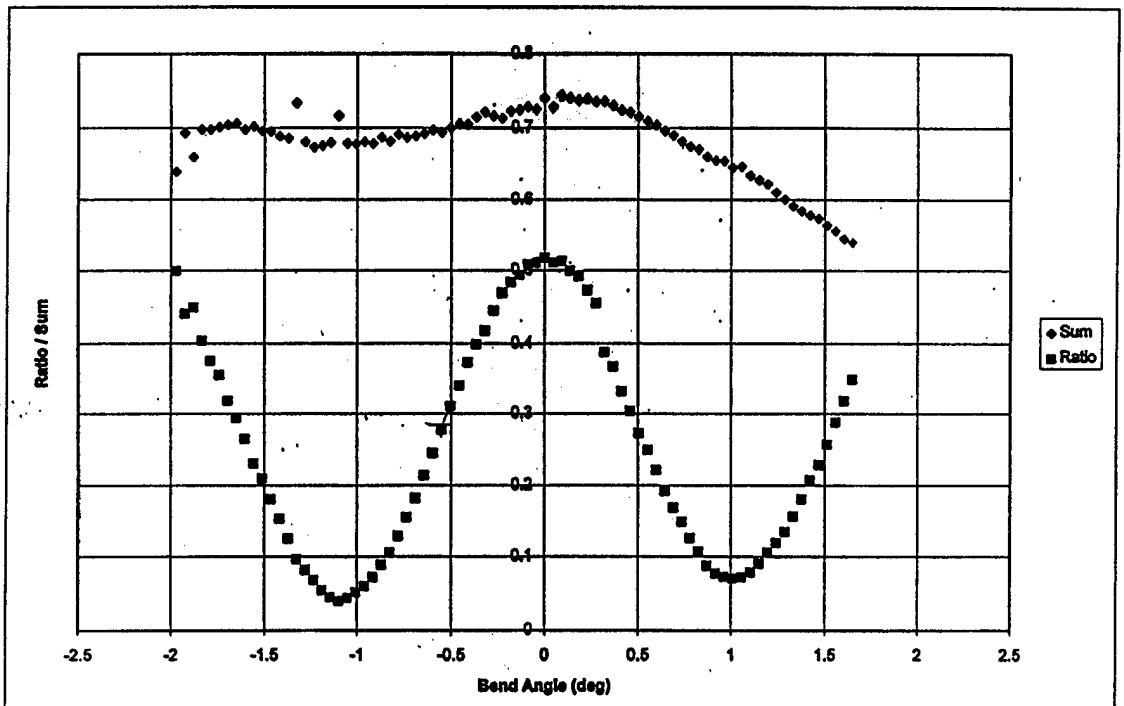

Figure 2 Bending Response of First Equipoint Coupler in Air

1. Starting with an axially aligned coupler (zero deflection) the coupling ratio varied with increasing bending as illustrated in Figure 2. Initially, the coupling ratio was always observed to decrease and then to vary cyclically as the bend angle progressed. This phenomenon is compatible with variation in the interaction length (beat length) for the two propagating optical modes as described in theory.[7]

2. Starting with an axially aligned coupler (zero deflection) the derivative of the coupling ratio as a function of the bend angle ($dR/d\Theta$) was initially zero. This means that for small signal detection, the axially aligned configuration was not optimum.

3. Starting with an axially aligned coupler (zero deflection) the bend response was symmetric about the zero deflection condition.

4. In all of the experiments, it was observed that initially the coupling ratio would decrease with increased bending. In the initial cycle, the coupling ratio can vary between the initial condition and zero.

The consequences of observations 2,3 & 4 were that a small prebend should occur in the interaction length (waist region) of the two fibers and that the configuration should be arranged so that the measurand would cause the bend angle to vary about a preset, biased condition with about 50% of the optical power in each of the output fibers. In addition, the coupler should initially be pulled to produce a 100% transfer of power to the other fiber since this signal level will be the maximum attainable without degenerate interpretation. This altered configuration was predicted to produce the highest small signal sensitivity and the highest linearity in the response.

5. During the experiments, it was observed that the bending response was complementary (variation in coupling rather than variation in loss) if the bending radius was symmetrically located in the center of the coupling region. Bending which occurred to either side, in the tapered region, produced significant loss. It was concluded that bending should be limited to the coupling region through modifications of the mounting hardware geometry.

Two sensor configurations were developed in accordance with the preceding results. (No illustrations to conserve space) In both of these designs, the fiber was pulled to the 100% coupling condition and then relaxed to the 50:50 condition while in contact with the RTV resin. That procedure was required because the sensor's coupling ratio is strongly affected by the index of refraction of the material which surrounds it and strongly changed as the potting material was added. By adjusting the radius of curvature of the prebend while it was in contact with the uncured potting material, the sensor was balanced to any preset ratio value.

The first of the two "bent fiber" configurations was the more robust. The fiber was suspended between two axial supports, allowing extension and contraction of the prebend which was freely suspended in uncured RTV resin.

The resin performed four functions. It coupled the sensing diaphragm to the fiber support and provided the mechanical path for the signal to act on the sensing fiber. It provided a mechanism for mechanical amplification of the measurand because of the ratio of contact areas from the sensing diaphragm and the fiber support. It increased the index of refraction surrounding the fiber interaction length thereby increasing the coupling and therefore the sensitivity of the element. It complexed with adsorbed water on the surface of the glass fiber and therefore prevented breakage of the fiber due to the action of water on any surface defects which may exist. (The failure mode for glass is invariably the propagation of surface flaws driven by tensile stress. This failure mode is known to be highly aggravated by the presence of H_2O on the fiber surface. Conversely, glass fiber is known to be one of the highest strength construction materials known and its use as a suspension element dates to the very earliest scientific apparatus.) Because of the suspension geometry of the fiber, it was free from any tensile stresses imposed by the input and the design was therefore very rugged.

The second design potted the prebent fiber in cured RTV as in the original concept, except that the bending region was physically limited by the physical supports to about 1 cm. at the fiber waist. The prebent fiber was fluid coupled to the sensing diaphragm, as before, and the same mechanism for mechanical amplification was provided. Since the fiber was subject to tensile stresses imposed by the physical constraints of the potting medium, this design was protected from breakage by snubbing the mechanical motion of the sensing element through physical contact with the back cover.

Both of the bent fiber sensor configurations were built. Both provided high quality outputs functioning as either an accelerometer (the sensor body acted as the proof mass freely supported by the sensing diaphragm) or as a pressure sensor (pressure acting against the sensing diaphragm with the sensor body supported). These sensor configurations also supported the hypothesis that limiting the bending to the waist region of the coupler would enhance variation in the coupling ratio and minimize the loss mechanism due to bending in its tapered regions. This feature enabled full implementation of the differential signal processing mode and added 3 dB to the Signal to Noise performance of the sensor relative to single line techniques.

Although both of these two designs worked well, both were physically very large devices (about 3 in dia.) which was driven by the need to support and pot the exposed fiber of the coupler. To minimize the size of the devices, a radically different approach was required.

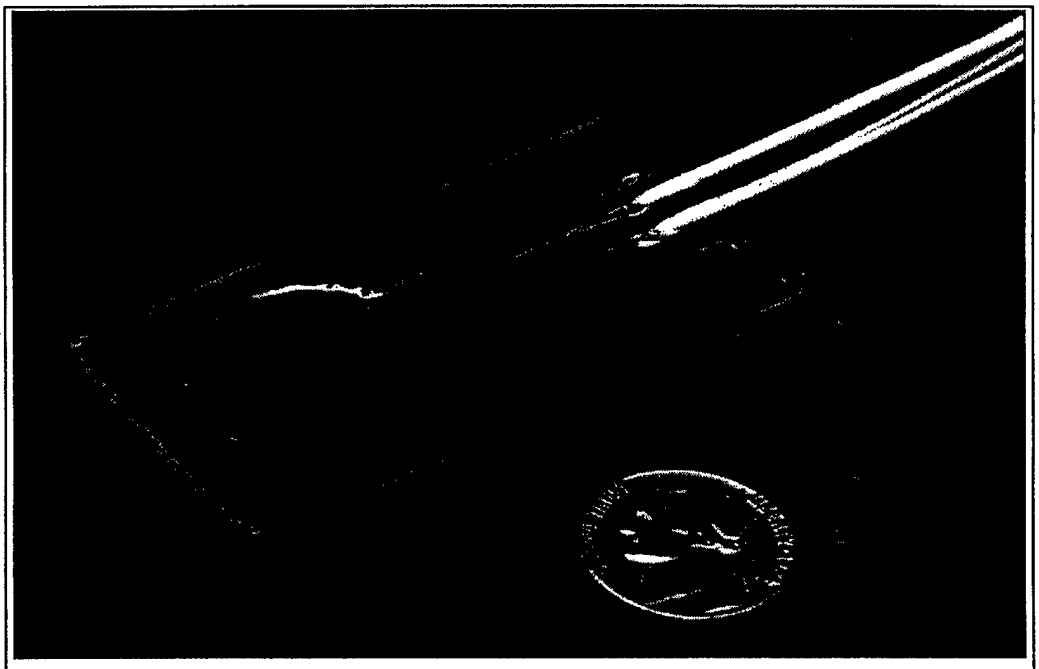

Figure 3 Proposed Design (larger configuration) of the wrist sensor using fiber loop construction

For the proposed configuration, it was clear that miniaturization of the sensor would require that the entrance and exit fiber must physically occupy the same space. i.e. the fiber must be folded back on itself. When this was attempted, the bending occurred primarily in the waist region where the fiber had the smallest bending cross section. If the fibers were pulled in air to reach 100% coupling (full transfer of the optical power to the other fiber), folded back on itself, and then immersed in the liquid potting resin, it was found that a fully active coupling alignment which produced a 50:50 division of power could be found and that the losses for the configuration were no higher than in the axially aligned configuration. This configuration was constructed in several sizes which match the contact requirements of the contact on the body. The sensor configuration illustrated in Figure 3 is designed for the brachial pulse and is slightly larger than the wrist pulse design, i.e. 18 mm vs 13 for the wrist. The features are more distinct in this photograph.

The loop sensor configuration enabled construction of a sensing diaphragm as small as 13 mm. diameter to enclose the tip of the coupler loop. The entrance and exit tapers were firmly supported by the sensor frame which formed the backbone for support and placement of the sensing diaphragm over the radial pulse point. Contact pressure required for sensing was very light, being compatible with the pressure required to keep the device in place. This is comparable with the pressure produced by an elastic band used to support a wristwatch.

Figure 11 (Phase I --Task 5) illustrates the radial pulse measurement taken from one of the program scientists using direct contact between the sensing diaphragm and the radial pulse point with no mechanical amplification. Figure 12 illustrates the FFT taken from that pulse signature. The FFT trace is the ensemble average of 10 x 1024 point FFT calculations. It illustrates the pulse rate at 1.5 Hz (90 beats per minute), breathing rate at 0.4 Hz (24 breaths per minute), and demonstrates the signal bandwidth (discernible above noise to about 20 Hz). The relative Signal Amplitude represents almost full scale for the circuitry whose measured S/N is about 74 dB.

TASK 2 -- Transition to 1300 nm Light Emitting Diodes (LED's):

The transition to 1300 nm was relatively simple. The task required selection of fiber type, source type, and detector.

Fiber

Fiber selected was the Corning SMF28 which has been used by the experimenters for many years. It is the industry standard for telecommunications supporting transmission in both the 1300 and 1500 nm low loss windows. This fiber is of the step index type and has supported coupler manufacture by the experimenters which are routinely below 0.5 dB excess loss. This is a very high quality coupler compared to industry standards.

Sources (LED vs. LD)

Both Laser Diode and Light Emitting Diodes are available for 1300 nm. Although the task had correctly selected the LED type, that choice was not fully supported from a technical point of view and a review of the relative qualities of the two types was performed.

At 1300 nm. the Laser Diode is a little cheaper, and considerably more efficient than the LED. Typical devices offer 1 to 2 mw of power in the fiber with drive currents of about 25 ma. Noise sources include shot noise in the emission process, 1/f noise due to current conduction across the PN junction, destabilization of the resonant cavity due to back reflection of coherent radiation from the fiber end, and mode hopping (a stepwise change in the resonant conditions in the cavity as frequency varies with the drive current and junction temperature). The laser usually offers a method of stabilization using the small photodetector inside the device to control the emission power. This detector senses emission power by detecting the light leakage from the back face of the Fabry Perot resonant cavity.

The LED is considerably less efficient than the LD. Typical devices offer 100 to 150 μw of radiation in the fiber with drive currents of 50 to 60 ma. The LED has lower spectral purity, but its emission frequency varies smoothly and almost linearly with the drive current and shows no discontinuities in the emission power or frequency.

Both devices suffer from frequency drift due to variations in the junction temperature and respond to temperature control. This is usually implemented by inclusion of a small thermoelectric cooler mounted just under the emitting device and inside the physical package. This cooling, however, uses considerable current to drive the TEC device and considerably affects the electrical efficiency and thus the battery life. If it can be avoided, this is a considerable gain.

Selection of the source type was based entirely on noise content in the output signal without significant control measures. The LED has no back facet detector and was tested with current control only. The LD has a back facet detector and was thus tested using both power control and current control modes. The results are illustrated in the following three plots of the measured Power Spectral Density in the output.

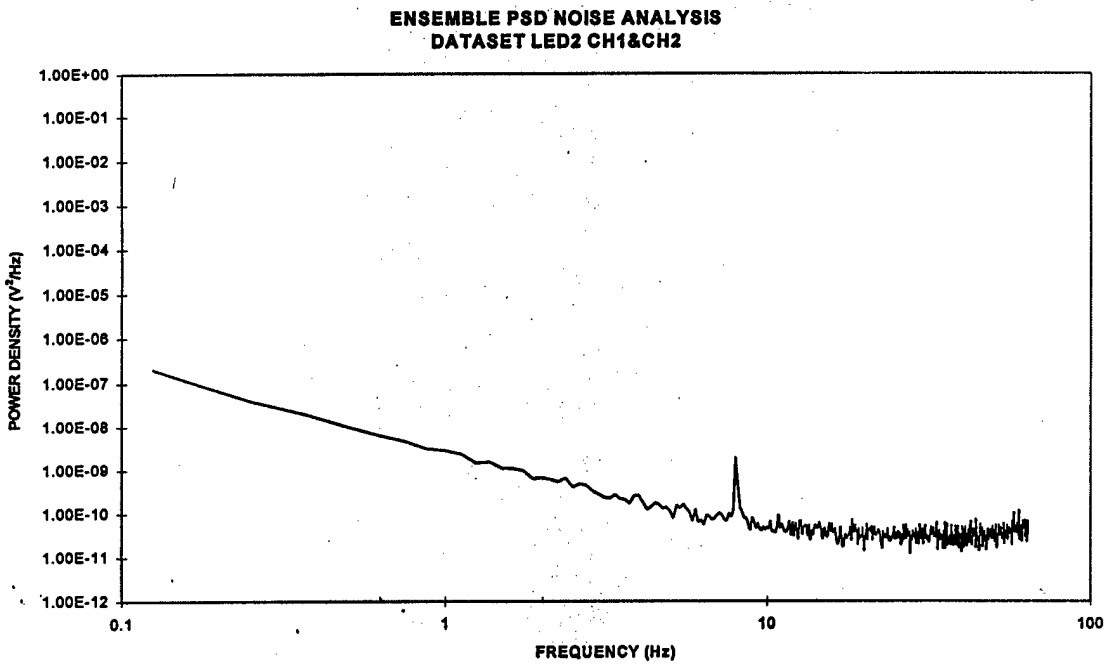

Figure 4 Noise Content in Output from LED using Current Control

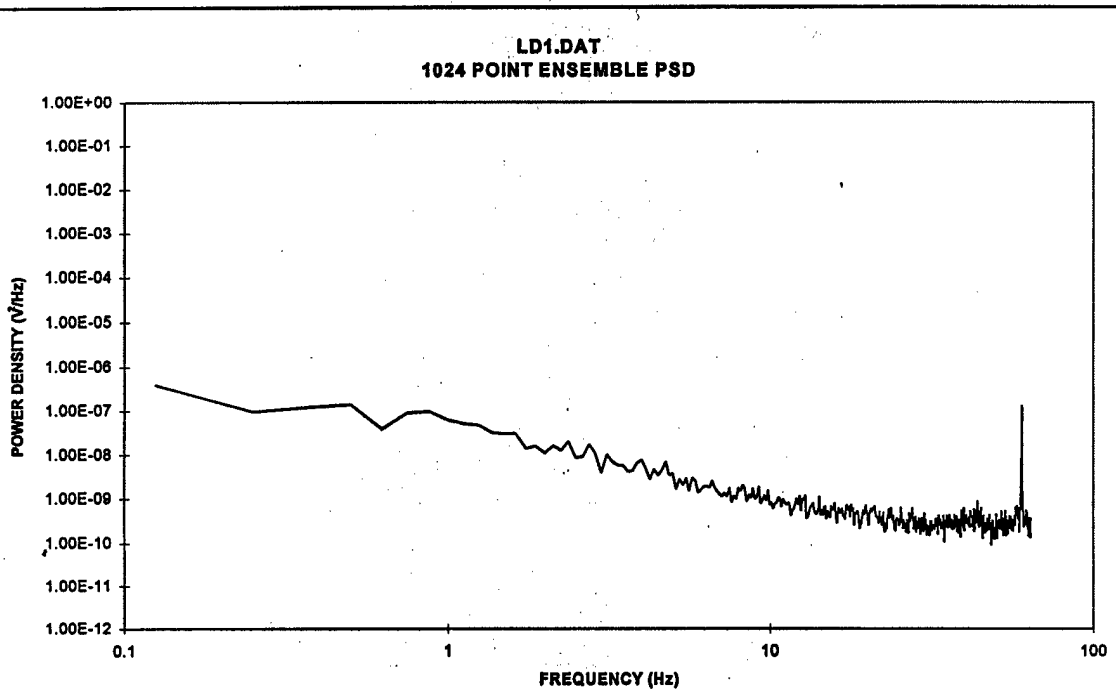

Figure 5 Noise Content in Output from Laser Diode using Current Control

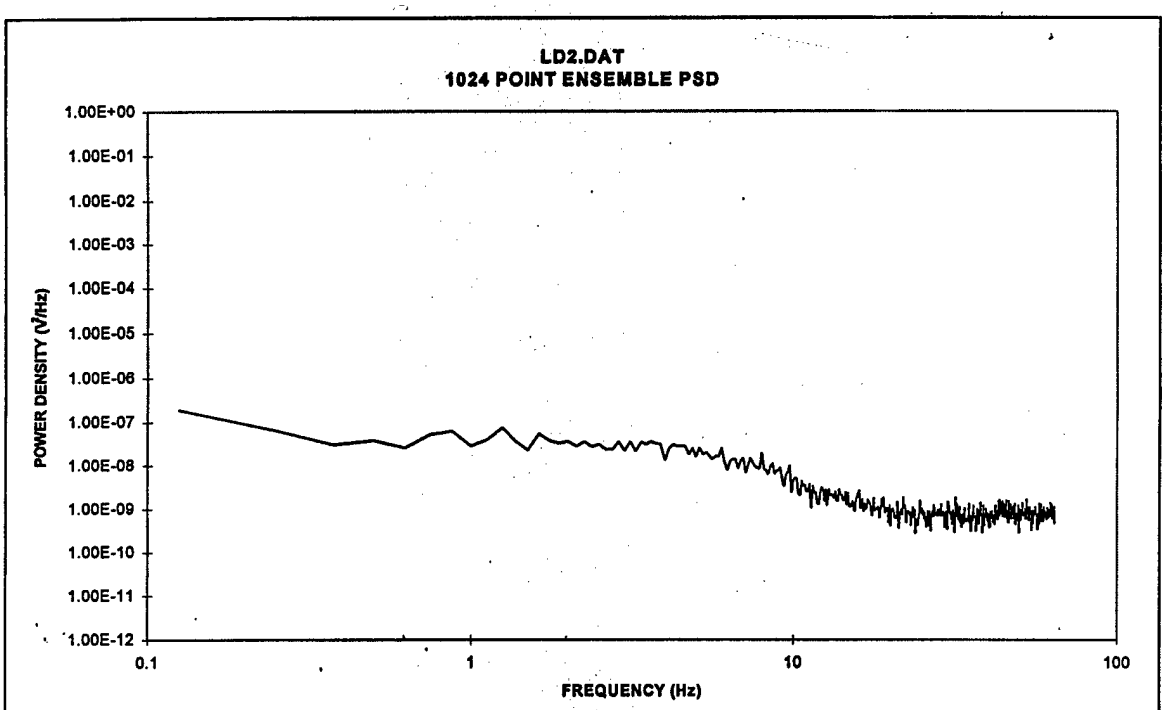

Figure 6 Noise Content in Output from Laser Diode using Feedback from the Photo Detector

When the PSD's were integrated over the signal bandwidth of 64 Hz, the results were clear. The LED, with its lower power, produced about 80 dB of available signal to noise compared to only 50 - 55 dB available from the Laser Diode. The LED required only simple current control to achieve this capability. This subject should be revisited in the phase II effort because, if the laser can be suitably controlled through proper design of the power feedback circuit, it offers a factor of two reduction in power requirement and a factor of ten improvement in the light power available. The higher power level should produce another 10 dB of available signal to noise.

The noise contained in the PSD's is of the 1/f type. Since it will be present in the same proportion on both channels of the sensor device and since it is of very low frequency, it will respond to simple difference over sum processing and can be removed.

Detector

Detectors in general use at 1300 nm are either derived from GErmanium or from Indium Gallium Arsenide. The InGaAs devices have generally replaced the older Ge types because of higher conversion efficiency and higher shunt resistance. They therefore result in lower noise when combined with the transimpedance devices of the following preamplifier stage. The cause will become clearer in the discussion of the next task.

Detectors can be connected in either the PhotoVoltaic or the PhotoConductive modes. In the PC mode, a reverse d.c. electrical bias is placed on the diode which has two effects. It reduces the junction capacitance by increasing the separation of charge carriers at the junction and it increases the transit time for charge created by the incident light signal. The result is a significant increase in the frequency capability of the device at the expense of noise created by charge leakage across the junction. This "dark current" is a function of the electrical bias, not the incident light, and it contaminates the signal quality for very low frequency applications such as the current design. The PV mode of operation simply observes the current created in the device by incident light. It suffers from loss of linearity and noise if the charge is allowed to accumulate and back bias the junction. The solution to both problems is the transimpedance configuration of the preamplifier which clamps the voltage across the diode to zero.

Noise created in the PV detector is solely due to the statistics of the occurrence of independent photon events. The resulting "shot" noise is the fundamental limit of the technique and it is classically represented as:

$$i_{shot} = \sqrt{2eI_oB}$$

where:

i_{shot} is the rms value of the noise current in amperes (rms)
e is the charge on an electron = 1.6 x 10-19 coulombs
I_o is the photon current produced in amperes
B is the bandwidth in Hz

As shown in the next section, the receiving portion of the circuit is capable of greater than 120 dB of Signal to Noise predicated on this noise source alone.

TASK 3 -- Design and Construct several electronic interface units:

The function of the Electronic Interface Unit (Optical Receiver) was to provide the electrical interface between the optical receivers (InGaAs diode detectors) and the modulation circuit of the low power transmitter (Voltage Controlled Oscillator) which is to be used to downlink body motion, pulse, and breathing rate information to the belt or helmet mounted intermediate communication device. The technical objectives of this task were to obtain a clean, low noise electrical signature of the desired measurand and to provide an output voltage capable of controlling the VCO circuit without contamination of the Signal / Noise present in the optical signal.

The electrical circuit for the Optical Receiver (EIU) is presented in Figure 7. It was comprised of two identical parallel paths, one for each of the differential input lines from the optical sensor. The first stage was the transimpedance amplifier which received the optical signal and established the noise figure for the remaining circuits. Since the output of the transimpedance amplifier had a strong d.c. bias due to the average optical power on the line (the optical carrier) a second stage, buffer amplifier, was required to

remove the d.c. bias component so that further signal amplification was possible without running the signal output into the power supply rails. D.C. coupling was used in this simplest configuration in order to avoid the implicit differentiation associated with the a.c. approach. The UAF42 was an active three pole filter which can be adjusted to remove high frequency components which alias into the FFT or PSD analytical results. Sum and difference amplifiers provided a means to perform difference over sum processing which was included to remove the low frequency 1/f noise components.

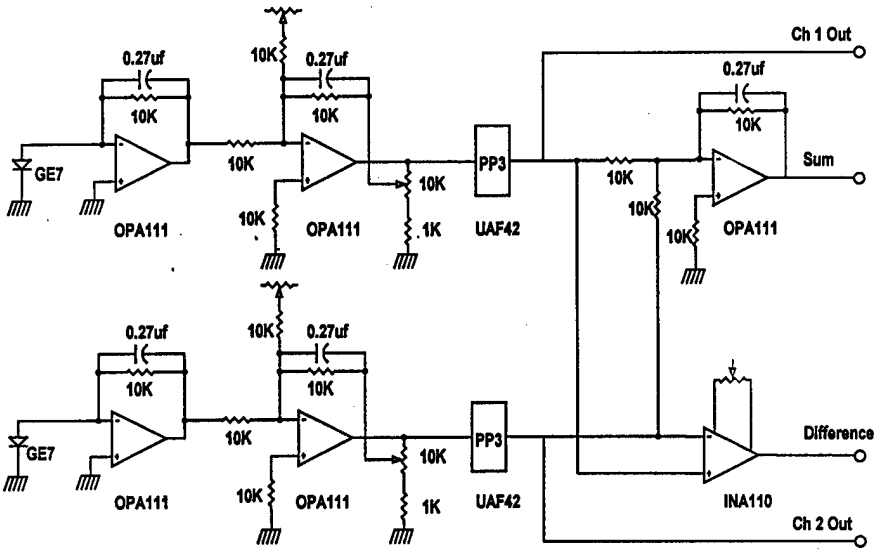

Dual Channel Transimpedance Preamp for Optical Signal Conversion

Figure 7 Circuit of the Optical Receiver and Analog Signal Processing Elements

The optical interface was provided using a traditional transimpedance amplifier design to receive the photocurrent from the photodetectors which were used in the Photo Voltaic mode. Since the transimpedance amplifier clamps the photodiode bias to zero volts, this mode completely eliminates dark current and its 1/f noise contribution to the total noise.

The total noise at the output from the operational amplifier can be calculated as:

$$e_{nt} = Z_f \left[\left(\frac{e_{n_a}}{Z_s} \right)^2 + i_{n_a}{}^2 + i_{n_{sh}}{}^2 + i_{n_f}{}^2 \right]^{\frac{1}{2}}$$

where:

$$Z_f = R_f \left[1 + \left(\omega C_f R_f \right)^2 \right]^{\frac{1}{2}}$$

$$Z_s = \frac{R_{sh}}{\left(1 + \left(\omega C_j R_{sh} \right)^2 \right)^{\frac{1}{2}}}$$

$$i_{n_{sh}} = \left(\frac{4\,kT\Delta f}{R_{sh}} \right)^{\frac{1}{2}}$$

$$i_{n_f} = \left(\frac{4\,kT\Delta f}{R_f} \right)^{\frac{1}{2}}$$

In the equations, R_{sh} and C_j are the shunt resistance and junction capacitance of the detector (50 MΩ and 80 pf). R_f and C_f are the Resistance and Capacitance in the amplifier feedback path. k is Boltzmann's constant (1.38 x 10-23 joules/K). Δf is the width of the passband. T is the absolute temperature in degrees Kelvin.

Since the noise components are random, their powers add, not their amplitudes. The equation calculates the rms noise contributions from the amplifier's voltage and current noise characteristics, and the Thermal noise (Johnson noise) contributions from the shunt and feedback resistance.

The equation demonstrates the sources of electronic noise in the interface circuit and leads selection of the electrical devices. Comparison of the rms noise voltage with the rms shot noise produced by the conversion of the optical signal establishes the theoretical Signal / Noise capability of the circuit.

The Burr-Brown OPA111 low noise precision difet operational amplifier was chosen as the input device due to its exceptionally low current noise characteristics.

The MRV Communications MREDSP015-1 LED was selected to supply the 1300 nm illumination which supplies 150 μw of optical power on the fiber. The GAP 1000 InGaAs photodetectors (replaced the GE7 devices) were selected as the optical receivers. These have an active area of 1mm, responsivity of 0.9 a/w, a junction capacitance, C_j, of 80 pf and a shunt resistance, $_{Rsh}$, @ 0 volts bias of 80 MΩ. Using a feedback resistance, R_f, of $10^4\Omega$, the output voltage will always be well within the power supply rails at the output of the op-amp transimpedance stage.

Using the components selected, the analysis illustrates that the Johnson noise contribution from the feedback resistance overwhelmingly dominates the electrical noise in the output of the op-amp and the shot noise contribution is larger by a factor of 5x. Based on the 150 μw of optical power on the line, the rms shot noise contribution in a 100 Hz passband can be calculated as:

$$e_{shot} = 0.65x10^{-6} \text{ vrms}$$

at the output of the amplifier. The signal swings between zero and max power on each of the signal channels, thus the maximum signal amplitude is 0.707 x the half amplitude:

$$\text{Signal} = 0.47 \text{ vrms}$$

The dynamic range available for the signal in the receiver is thus:

$$\text{Dynamic Range} = 117 \text{ dB}$$

Outputs from the circuit are the difference signal which contains the data, the sum signal which is the noise reference without signal, and the two independent channel outputs. Since the amplitude noise from the LED or LASER source is present on both channels in the same fixed proportion, dividing the channel outputs by the sum of both channels (the total power + 1/f noise components) results in removal of the common mode noise signals. Figure 13 illustrates the result using a very noisy (relatively speaking) Helium Neon gas laser. The signal to noise improvement is almost 60 dB at the low frequency end. As the frequency increases, the channel coherence begins to interfere with the method due to the slight phase differences which accumulate between the two channel paths.

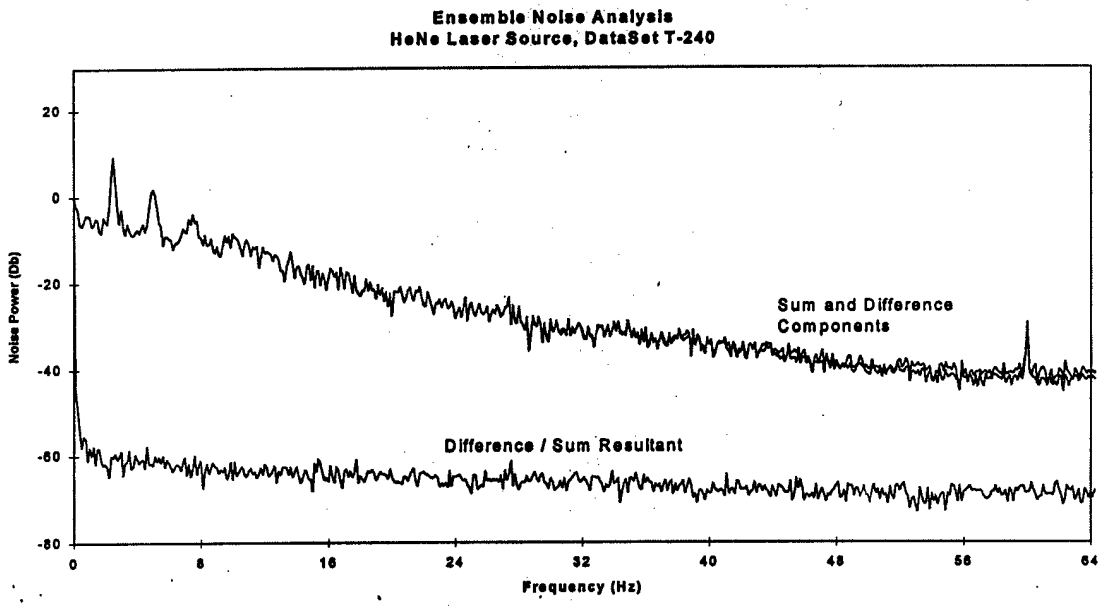

Figure 8 Ensemble Noise Analysis of a Very Noisy Gas Laser Demonstrating the Results of the Difference / Sum Signal Processing

Construction of the Hardware

Circuit boards for the laboratory test circuitry were drawn using Autosketch and were manufactured by WWW Electronics for ETC. The layout is very large to allow for considerable rework and testing of variations on the circuitry as the experiments require. The test apparatus contains offset bias adjustments and gain adjustments for two full devices (four channels) to allow the measurement of pulse wave velocity. A picture of the completed assembly is shown in Figure 9.

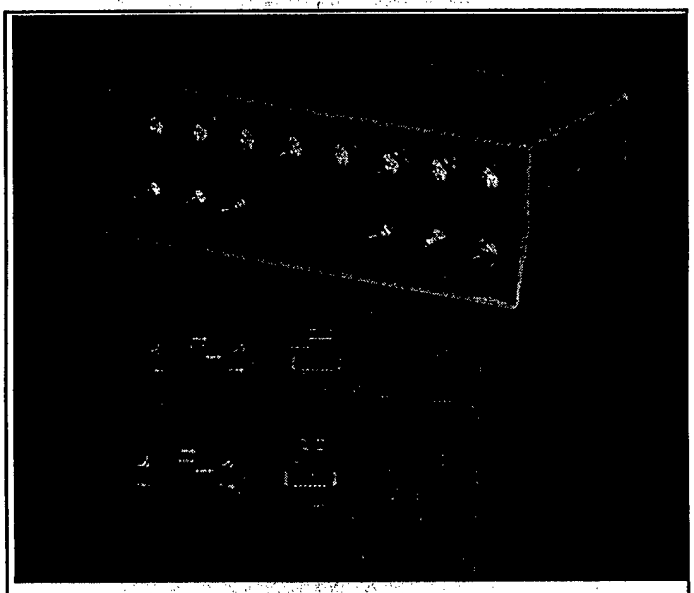

Figure 9 Electronic Interface Unit (Optical Receiver) and an unpopulated PCB

TASK 4 -- Data Logger Interface at the receiver side of the sensor/transmitter system:

The subtasks outlined under this part of the program in the Statement of Work were to 1. establish a computer-based data logging system, 2. perform the necessary signal processing to extract the heartbeat and respiration signals from the signal provided by the fiber optic coupler sensor, and 3. demonstrate the capability of transmitting signals using radio transmitter/receiver circuits.

All subtasks were performed. With regard to subtask 1. A portable computer has been equipped with a analog/digital (A/D) conversion board and programmed to perform the data logging and storing functions required.

With regard to subtask 2. no signal processing was found to be necessary as the signal measured by the fiber optic heartbeat sensors, even the earlier versions, was of such quality as to require no extraction to visualize the heartbeat and respiration signals. In fact, as a result of the high quality, further analysis of the data could be performed, such as Fast Fourier Transforms (FFTs), which provided additional insights into the spectral content of the sensor signals. Examples of raw heartbeat data streams and the corresponding FFTs are given under Task 5 (Test of the heartbeat/respiration sensor).

For subtask 3 the contractor was able to leverage the results of an ongoing microchip-based sensor program with the University of Virginia's Center for Custom Integrated Design, Oak Ridge National Laboratories' Health Services Division, and Empirical Technologies Corporation for this DARPA program. The feasibility of transmitting and receiving radio frequency signals, using the on-chip antenna on a microchip package measuring 4.6 x 6.8 mm manufactured through the DARPA MOSIS fabrication process, was demonstrated. The results of this microchip package program will be directly applicable to the micropackaging aspects of the Phase II part of this program.

Subtask 1: The data logger interface is based on a Toschiba Satellite 100CS notebook computer that is powered by a 75 MHz Pentium processor while the A/D interface is provided by a PCMCIA card (PCM-DAS 16D/16 from Computer Boards Inc.). The card is based on a 16 bit converter, providing a resolution of a part in 65536, and has programmable bipolar voltage ranges of ±10, ±5, ±2.5, and ±1.25 Volts. Furthermore the card supports acquisition rates up to 100 kHz.

The Logger software package was developed within the Microsoft Visual Basic 4.0 environment. Computer Boards Inc. provides a Visual Basic library of function calls to control the D/A card as well as a number of graphical interface units for the Windows © environment, such as an oscilloscope, which is capable of real-time data display updates.

The central idea in collecting fast data streams (several hundred Hertz or more) and displaying them in the slow Windows © environment (10 Hz or so) is to establish separate operations for the data collecting A/D board and the displaying computer. This is accomplished by launching the A/D board, which is equipped with its own processor, in a so-called background mode, whereby it operates independently of the computer which is running the displaying program in foreground. The two processes communicate through a buffer that resides on the A/D board. The board updates the buffer continuously with recorded data as well as an index that indicates how many data counts have been collected and which channel a given data came from. The Logger program running in the foreground accesses the buffer and reads out the section of data collected since the last readout which is handed to the Windows oscilloscope module for display.

The Logger system, in its present implementation, is capable of displaying and recording up to 4 data channels at rates ranging from 1 - 4 kHz, which is entirely sufficient for the requirements of this project. Increases to higher rates are possible but management of the sizable data buffers becomes difficult within the 16 bit environment supported by Windows 3.1. This factor also determines the length of the scan since the total buffer size cannot exceed 32,768 within a 16 bit environment. Windows 95 with its 32 bit support promises much better memory management capability.

Subtask 3: This part of the program demonstrated the feasibility of transmitting radio frequency signals, that could be broad band modulated, over a short distance such as 1 meter. The central problem in transmitting the heartbeat/respiration spectrum is that, while the transmission of signals corresponding to the human voice spectrum (about 20 Hz - 20 kHz) using radio AM or FM techniques is fairly straight forward, transmission of low frequency signals (around 1 Hz) is not. This is due to the fact that the frequency resolution requirement needed to demodulate a low frequency signal from a high frequency carrier becomes too high.

Both AM and FM techniques rely on modulating a high frequency carrier (about 1 MHz for AM, about 100 MHz for FM) with the signal to be transmitted. Both techniques produce, if the carrier and its modulation are examined in frequency space, sidebands above and below the carrier frequency. The frequency difference between the carrier and the sideband corresponds to the signal to be transmitted. The radio receiver has to demodulate these two signals in order to extract the sideband signal, amplify it, and drive, for instance, a speaker.

If the signal to be transmitted drops to 1 Hz or below, the corresponding sideband moves closer to the carrier, making it increasingly difficult for the receiver to demodulate the two signals, since the required frequency resolution has effectively increased by more than an order of magnitude. In fact, since even high fidelity systems are designed for at least 15 to 20 Hz signals, lower frequency signals cannot be demodulated. Consequently off-the-shelf radio technology, whether AM or FM, cannot be used for the transmission of low frequency signals.

A better technique, which is used in the mentioned microchip-based sensor University of Virginia/ETC program, is to first "shift" the low frequency signal to a higher frequency, thereby removing it from the highest 1/f noise regime, and to then modulate a high frequency transmission carrier to transmit the shifted signal. At the receiver side the shifted signal is demodulated from the carrier, and the original low frequency is then demodulated from the recovered shifted signal. Neither of the two demodulation processes place unreasonable resolution requirements on the circuitry. Specifically, the low frequency signal is shifted into the 70 - 200 kHz range using a voltage-controlled oscillator (VCO). This frequency is then used to modulate a 350 MHz transmission carrier that is fed via a high speed amplifier to the on-chip antenna.

A preliminary version of the circuit was fabricated in a 2.0 micron, twin-metal, twin-poly, N-well, BICMOS process technology provided by the DARPA MOSIS fabrication process. It was tested as part of the feasibility demonstration for transmitting signals in the 100 mHz range over a distance of 1 meter. Since the device, which measures 4.6 mm by 6.8 mm, was specifically designed for transmission tests, it contains three different antenna designs as well as the driver and oscillator circuitry. The ring oscillator was driven with voltages of 3.5 to 5 Volts, resulting in frequency modulations of 220 - 420 MHz in the carrier, as recorded using a spectrum analyzer with a dipole receiving antenna. The output power was varied from -5 dBm to 19 dBm, producing a recordable signal at the receiver end over the entire power range. The frequency spectrum results are given in Figure 10, which is a 30 MHz section of the recorded spectrum. The three peaks visible, at 405, 410, and 419 MHz are due to the slightly different resonant frequencies of the three physically different antennas. The second version of that chip, which incorporates the complete circuitry, including the VCO, was being returned from the MOSIS foundry at the time of this writing, and will permit testing of the low frequency modulation capability.

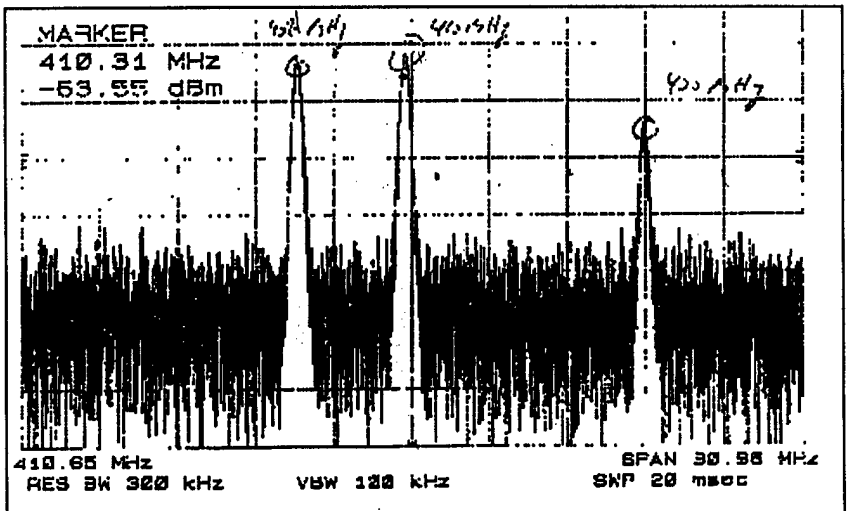

Figure 10 Emissions Spectrum Measured using the UVA designed Transmitter on a Chip

TASK 5 -- Test the heartbeat/respiration sensor:

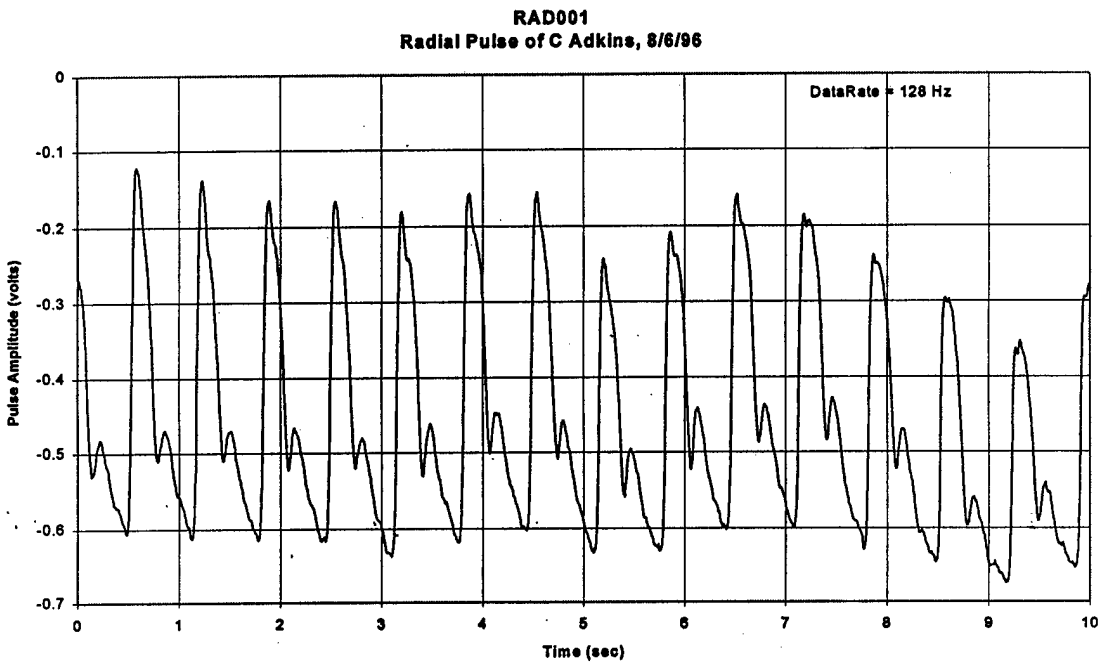

Figure 11 Radial Pulse Data Measured using the ETC Wrist Sensor (recorded at 128 samples per second)

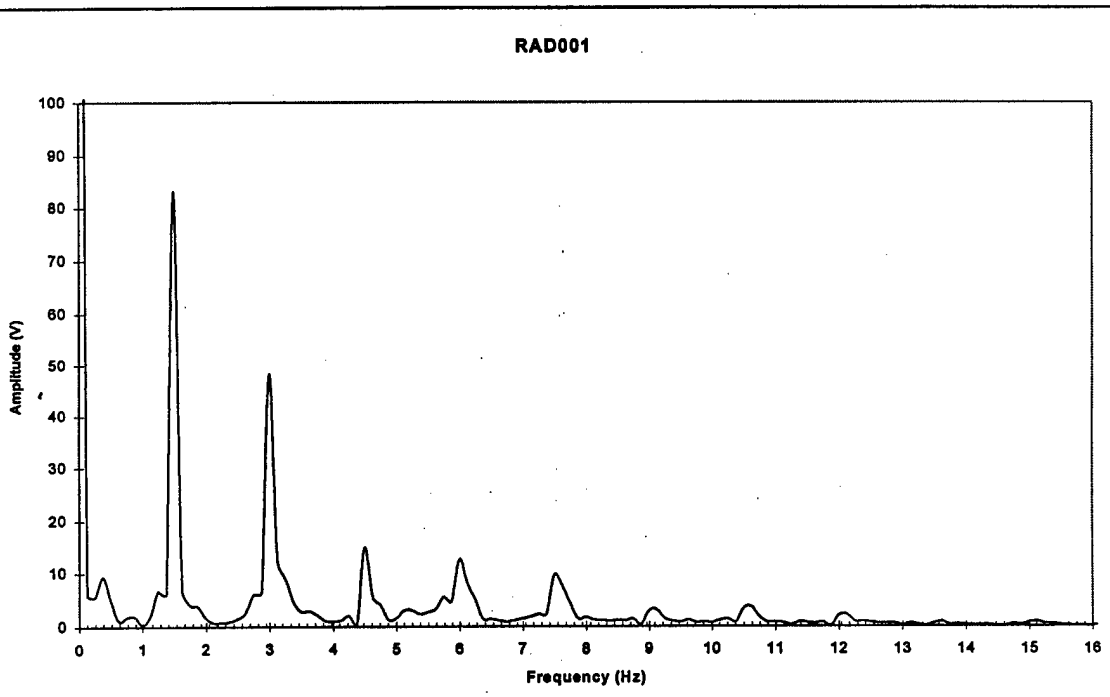

Figure 12 FFT of the Pulse Data recorded in Figure 12

A number of heartbeat/respiration data streams were obtained with several sensors configured in the looped-coupler configuration using project team members. The compact size of the device, whose sensing area is now about the size of a penny, made coupling particularly to the radial pulse pressure point far easier than with the previous sensor designs. Signals that could be viewed effortlessly on the data logger screen or an oscilloscope were obtained within seconds of applying the device. All measurements were taken with the subjects at rest, either standing or sitting. A wrist harness for maintaining the coupling contact between sensor and the pressure point could not be developed within the Phase I effort. The wristband assembly, along with an investigation of the high exertion heartbeat/respiration spectrum, will be undertaken as part of the Phase II effort.

Figure 11 is a sample of the raw data streams that were collected and establishes the high signal quality the sensor provides, which precluded the need for signal extraction techniques. Both the heartbeat signal as well as the slow respiration induced modulation on the data stream are clearly visible. In order to better quantize the spectral information of the time domain data, Fast Fourier Transforms (FFTs) were taken of the data. Figure 12 presents the FFT trace that is the ensemble average of ten 1024 FFT calculations, performed on ten consecutive 1024 point sections in the time domain data. The heartbeat pulse rate of is 1.5 Hz, corresponding to about 90 beats per minute, while the respiration signal is 0.4 Hz , or about 24 breaths per minute. The signal amplitude was almost full scale for the circuitry whose measured signal/noise ratio was about 74 dB.

Conclusions:

This Phase I effort has established the feasibility of a heartbeat and respiration sensor with high sensitivity, based on a fiber optic coupler, that will fit within the dimensions of a wrist watch. Radio frequency transmission test demonstrated the feasibility of using a custom designed integrated circuit with an on-board antenna and driver circuitry to transmit the sensor's low frequency signal to a receiver unit over a distance of one meter at frequencies of 220 - 420 MHz. Based on spectral information gained through Fast Fourier Transforms (FFT) and Power Spectral Density (PSD) calculations on actual heartbeat and respiration data collected with the coupler sensor, electronic interface were constructed. These units contain not only the opto-electronic conversion circuitry but also important filters and perform the sum and difference calculations needed to isolate the heartbeat-related components in the sensor's output signal. A laptop-based data A/D acquisition system was implemented.

List of Personnel:

Martin Baruch, Ph.D. is one of four members of the Board of Directors and is the Chief Scientist at Empirical Technologies Corporation. Dr. Baruch took advanced degrees in Mathematics and Physics (BS) from Hobart College and Molecular Physics (PhD) from the University of Virginia. Dr. Baruch was principal investigator for the program.

Charles M. Adkins, Ph.D. is one of four members of the Board of Directors and is the Chief Engineer at Empirical Technologies Corporation. Dr. Adkins took advanced degrees in Electrical Engineering (BEE) from Vanderbilt and Materials Science (MS & PhD) from the University of Virginia.

David W. Gerdt, Ph.D. is one of four members of the Board of Directors and is the President of Empirical Technologies. Dr. Gerdt took advanced degrees in physics(M.S) and materials science (Ph.D.) from the University of Virginia. His undergraduate degree is in physics from Southern Illinois University at Edwardsville. He is the inventor of the coupler/sensor technology.

References:

[1] Gerdt, D.W., and Gilligan, L.H., USP #4,634,858, Jan. 6, 1987.

[2] Kawasaki, Kawachi, Hill, and Johnson, A Single-Mode-Fiber Coupler with a Variable Coupling Ratio, Journal of Lightwave Technology, Vot. LT-1, March 1983, pp. 176 - 178.

[3] Murakami, Coupling between curved dielectric waveguides, Applied Optics, Vol. 19, No. 3, February 1980, pp 398 - 403.

[4] Murakami, and Sudo, Coupling Characteristics measurements between curved waveguides using a two-core fiber coupler, Applied Optics, Vol. 20, No. 3, February 1981, pp. 417 - 422.

[5] Gerdt, D.W., Final Report of the Thick Membrane Variable Coupler Fiber Optic Hydrophone Development, prepared for NADC under Contract N62269-88-C-1170 to Sperry Marine Inc., October 1989.

[6] Gerdt, D.W., Final Report of the Thick Membrane Variable Coupler Fiber Optic Hydrophone Prototype Test and Evaluation, prepared for NUSC under Contract N66604-88-M-G758 to Sperry Marine Inc., November 1989.

[7] Adkins, C.M., Final Report of the Fiber Optic Hydrophone Array Development Program, Report No. JA-24-5326, Contract No. N62269-90-C-0538, 24 May 1991.